Biosensors and Bioelectronics 87 (2017) 566–571

Contents lists available at ScienceDirect

Biosensors and Bioelectronics

journal homepage: www.elsevier.com/locate/bios

MnO_2 nanosheet-assisted ligand-DNA interaction-based fluorescence polarization biosensor for the detection of Ag^+ ions

Liang Qi [a], Zhe Yan [b], Yuan Huo [a], Xiao-Man Hai [a], Zhi-Qi Zhang [a,*]

[a] Key Laboratory of Analytical Chemistry for Life Science of Shaanxi Province, School of Chemistry and Chemical Engineering, Shaanxi Normal University, Xi'an 710062, China
[b] School of Materials Science and Engineering, Shaanxi Normal University, Xi'an 710062, China

ARTICLE INFO

Article history:
Received 29 June 2016
Received in revised form
17 August 2016
Accepted 26 August 2016
Available online 27 August 2016

Keywords:
MnO_2 nanosheets
Ligand-DNA interaction
Fluorescence polarization
Ag^+ ions

ABSTRACT

Silver (Ag^+) ions are highly toxic to aquatic organisms and accumulate in the human body via the food chain. Therefore, the development of sensitive and selective quantitative analytical methods for detecting trace amounts of these ions is necessary. In the present study, a MnO_2 nanosheet-assisted, ligand-DNA interaction and fluorescence polarization-based method was developed, for the first time, for sensitive detection of Ag^+. The addition of Ag^+ to the preformed proflavine-DNA complex induced the release of proflavine, which elicited weak changes in fluorescence polarization. The subsequent addition of MnO_2 nanosheets magnified the observed changes, making this a feasible method for the detection of Ag^+. The calibration graphs indicated good linearity over the concentration ranges of 30–240 nM for Ag^+, with a detection limit (S/N=3) of 9.1 nM. This method additionally exhibits high selectivity. The mechanism underlying the changes in fluorescence polarization caused by the addition of Ag^+ in the presence of MnO_2 nanosheets was further explored in this study. These findings demonstrate that the present MnO_2 nanosheet-assisted fluorescence polarization biosensor may represent a promising tool for the detection of Ag^+ ions. The results for practical detecting Ag^+ proved that this biosensor can be applied to environmental water sample analysis.

1. Introduction

Elucidation of the interactions between small ligands and biomacromolecules, such as plasma proteins (Cubrilovic and Zenobi, 2013; Wang et al., 2011), enzymes (Jang et al., 2013; Sakabe et al., 2013), and nucleic acids (Murata et al., 2013; Qi et al., 2015), provide new insights into biological activities and enable the development of novel compounds capable of efficiently regulating specific biological processes. In recent years, the interactions between fluorescence intercalators, such as PicoGreen and thiazole orange, and DNA have been utilized for the detection of a much wider range of targets (Pang et al., 2015; Tan et al., 2012). The binding of proflavine, a classical intercalator, to DNA has also been widely studied (Neidle et al., 1988; Tang et al., 1990); this compound is recognized as a Rev inhibitor that targets HIV-1 Rev response element (RRE) RNA at the Rev binding site (DeJong et al., 2003). Very recently, the interaction between proflavine and G-Quadruplex DNA was illustrated, with proflavine utilized as the indicator (Kumar et al., 2014).

The silver ion (Ag^+) is a common form of silver. As a highly bioactive cation, Ag^+ exhibits strong antimicrobial activity at low concentrations (Lai et al., 2010); however, high levels of Ag^+ exert serious biological effects on human health. This ion is additionally known to accumulate in the human body via the food chain (Morgan and Wood, 2004). Therefore, much attention is currently devoted to the development of methods for the accurate detection of trace amounts of Ag^+ (Zhu and Zhang, 2014); in particular, efforts have been made to develop fluorescent (Gao et al., 2015; Lee et al., 2015; Sun et al., 2013; Yang et al., 2015a), colorimetric (Li et al., 2009; Liu et al., 2012), chemical (Jiang et al., 2015; Kumar et al., 2011) and electrochemical sensors (Lin et al., 2011; Mensah et al., 2014; Xu et al., 2014; Yang et al., 2015b) for assays of Ag^+.

Fluorescence polarization (FP), which is commonly used for studying intermolecular interactions (Choi et al., 2012), is also an attractive technique for the detection of various targets (Huang et al., 2012, 2014; Ye and Yin, 2008). This technique may be utilized in combination with other commonly used nanotechnologies to obtain an enhanced FP signal, thereby enabling improved sensitivity of detection. Layered nanomaterials, such as graphene oxide, WS_2, and MoS_2, which possess unique physical and chemical properties, are utilized as FP signal enhancers in DNA-based

* Corresponding author.
E-mail address: zqzhang@snnu.edu.cn (Z.-Q. Zhang).

http://dx.doi.org/10.1016/j.bios.2016.08.093
0956-5663/

sensors (Shi et al., 2011; Yuan et al., 2014a; Zhu et al., 2013); furthermore, graphene oxide has been utilized in enhanced fluorescence anisotropy sensors (Yu et al., 2013; Zhen et al., 2015). Specifically, the thickness of MnO_2 nanosheets consisting of an edge-shared MnO_6 octahedral crystal lattice is of the order of nanometers or smaller, with lateral size ranging from submicrometers to micrometers (He et al., 2014). MnO_2, a well-known transition-metal oxide, has been widely studied, and MnO_2 nanoplatforms have been developed for biosensing applications (He et al., 2014; Yuan et al., 2014b; Zhang et al., 2014).

Proflavine recognizes the cytosine-guanine (CG) base-pair in the DNA double helix. Ag^+ is known to specifically bind cytosines to form a stable mismatch base pair of cytosine-Ag^+-cytosine (C-Ag^+-C) (Ono et al., 2008); recently, Swasey et al. revealed Ag^+ was also able to form another mismatch pairing of G-Ag^+-G, and this base pair showed higher stability than Watson-Crick C-G pairing (Swasey et al., 2015). Therefore, Ag^+ is considered to interfere, directly or indirectly, with the binding of proflavine to DNA. This proflavine-DNA interaction-based detection model, with proflavine as a fluorescence polarization indicator, does not suffer from limitations owing to unnatural folding and the formation of biomacromolecular structures, which is a limitation of detection methods utilizing fluorescent covalent labeling and surface immobilization (Umemoto et al., 2012). To the best of our knowledge, the present study is the first to explore MnO_2 nanosheet-assisted measurement of fluorescence polarization for the detection of Ag^+ (Fig. 1).

2. Experimental section

2.1. Chemicals and solvents

DNA oligonucleotides with the sequence 5′-TGTCGTCGTCGTCAAAAGTCGTCGTCGTC-3′ were custom-synthesized by Shanghai Sangon Biotechnology Co. Ltd. (Shanghai, China). Proflavine Sulfate Hydrate was purchased from Spectrum Chemical Mfg. Corp. (USA). All other reagents of analytical grade were commercially available and used without further purification. All the buffers were prepared with ultra-pure MilliQ water (resistance > 18.2 MΩ cm^{-1}).

2.2. Preparation of MnO_2 nanosheets

Bulk MnO_2 was synthesized using a previously reported method (Peng et al., 2013). Typically, 20 mL of a mixed aqueous solution of 600 mM tetramethylammonium hydroxide (TMA · OH) and 3 wt% H_2O_2 was added to 10 mL of 0.3 M $MnCl_2 \cdot 4H_2O$ aqueous solution in 15 s. The solution turned dark brown in color immediately upon addition of the mixed aqueous solution. Then, the solution was vigorously stirred overnight in the ambient atmosphere at 25 °C. After this mild oxidation reaction, the precipitate was washed with water and methanol and centrifuged at a very low speed of 2000 rpm for 20 min, after which the precipitate was dried in a vacuum oven at 60 °C. Finally, 10 mg of bulk MnO_2 was added to 20 mL of water for ultrasonic treatment. After ultrasonic treatment for 10 h, the dispersion was centrifuged at 1000 rpm, removing the un-exfoliated residues from the dispersion.

2.3. Detection of Ag^+

An ammonium acetate-buffered saline solution (20 mM, containing 20 mM NaCl, pH 7.0) was used for the detection of Ag^+. A mixture of proflavine (600 nM) and DNA (100 nM) was incubated at room temperature for 5 min. Various concentrations of $AgNO_3$ (6 μM) were then added and incubated for 30 min, followed by 6 μL of MnO_2 nanosheets (2 mg mL^{-1} in water), to a final volume of 150 μL. The adsorption time was 10 min.

In the selectivity assay, 11 additional representative metal ions (200 nM) were added for incubation for 30 min respectively, and 6 μL of MnO_2 nanosheets (2 mg mL^{-1} in water) was added for the

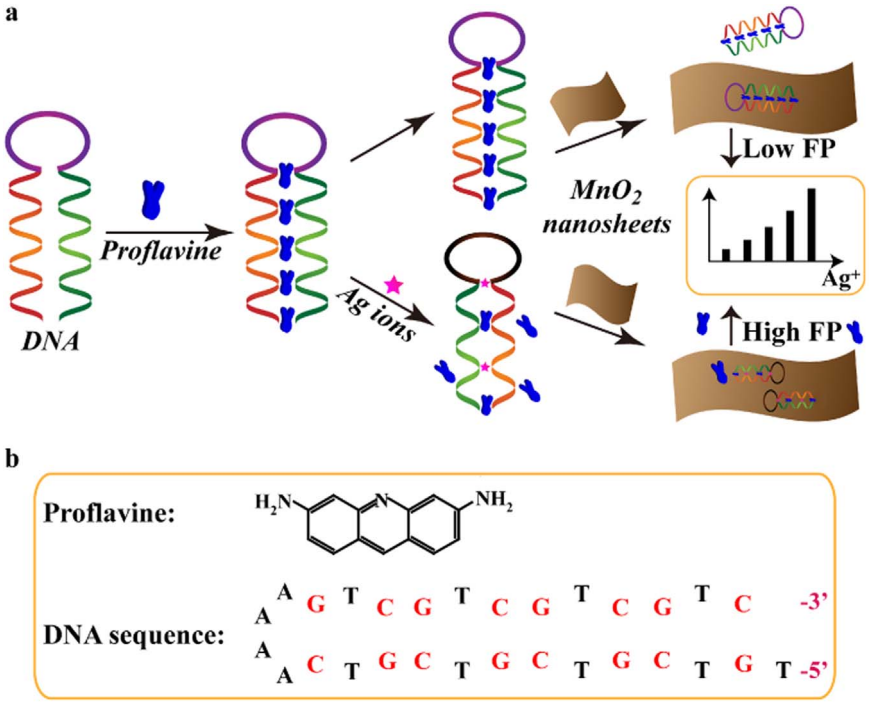

Fig. 1. (a) Illustration of MnO_2 nanosheet-assisted ligand-DNA interaction-based fluorescence polarization sensor for detection of Ag^+ ions. (b) Secondary structure of proflavine and DNA used in the biosensor. The secondary structure of DNA was predicted by the software "RNAstructure, version 5.7", with the parameters of max % Energy difference: 10, and Max number of Structures: 20.

measurement of fluorescence polarization.

In the analysis of real samples, tap water and lake water were firstly filtered through a 0.45 μm membrane, and the filtrates were stored at 4 °C. Three spiking levels of 50, 100 and 200 nM were set up and the standard solutions were added to the real samples to measure and calculate the recoveries.

2.4. Measurement of fluorescence polarization

Fluorescence polarization analysis was performed using an LS 55 Fluorescence Spectrometer at the excitation and emission wavelengths of 445 nm and 505 nm, respectively, with a slit bandwidth of 10 nm. The integration time was 1 s. Fluorescence polarization was measured at 505 nm for quantitative analysis. All fluorescence polarization values (1 P = 1000 mP) were read at least 5 times, which was calculated using the following equation, as described previously (Ye and Yin, 2008):

$$mP = 1000\frac{I_{vv} - GI_{vh}}{I_{vv} + GI_{vh}}$$

I_{vv} and I_{vh} are the fluorescence intensity horizontal to and vertical to the excitation plane, respectively, and $G = I_{hv}/I_{hh}$.

2.5. Measurement of UV–vis spectra

The excitation wavelength for proflavine (200 μM) was set at 445 nm, and the absorption spectrum of MnO_2 nanosheet materials (200 μg mL^{-1} in water) was scanned from 200 nm to 700 nm, as determined using an Evolution 220 UV–vis spectrophotometer (Thermo Fisher Scientific Inc., USA) using a 500-μL-volume quartz cuvette. The slit bandwidth was set at 1 nm and the scanning speed was set to low.

2.6. Circular dichroism (CD) measurements

Circular dichroism (CD) spectra of DNA, in the absence and presence of Ag^+, were measured using a Chirascan CD spectrometer (Applied Photophysics Limited Co., United Kingdom) with a quartz cuvette of 0.2-cm path length. The scanning speed was set at 200 nm min^{-1} and optical path at 1 mm. The CD spectra were obtained with correction for emission due to the buffer.

The DNA-Ag^+ complex was mixed thoroughly and incubated at 20 °C for 30 min in ammonium acetate buffer before testing. All CD spectra scans were repeated at least 3 times.

2.7. X-ray diffraction (XRD) characterization

XRD characterization was performed using a Rigaku X-ray Diffractometer (D/Max-3c, Japan). The Cu Kα radiation was at a wavelength of 1.542 Å. The data were collected from 5° to 75°.

2.8. Electron microscopy characterization

The samples were prepared on carbon-film-covered copper grids and images were obtained using a Tecnai G2 F20 Transmission Electron Microscope (TEM) at 200 kV.

2.9. Measurement of zeta potential

Measurements of zeta potential were performed using a Delsa™ Nano particle and Zeta potential analyzer (Beckman Coulter, Inc.), which is capable of measuring the zeta potential of nanoparticles at low concentrations or in turbid samples.

3. Results and discussion

3.1. Characterization of MnO_2 nanosheets

The synthesized MnO_2 nanosheets were first examined. The exfoliated MnO_2 nanosheets showed maximum absorption at ~371 nm, and the aqueous solution showed good dispersibility (Fig. S1, Supplementary material). The crystallographic structure was determined by powder X-ray diffraction (XRD); significant XRD peaks were recorded at $2\theta = 12.12$, 24.12, 36.16, and 65.54 (Fig. S2a). The zeta potential measurements showed that the MnO_2 nanosheets possessed a negatively charged surface (−147.36 mV, Fig. S2b). The transmission electron microscopy pattern showed lamellar structure of the MnO_2 nanosheet (Fig. S3). All these results from the characterization indicated that the synthesized MnO_2 nanosheet was qualified for the following Ag^+ sensing analysis.

3.2. MnO_2 nanosheet-assisted fluorescence polarization biosensor

We then investigated whether MnO_2 nanosheets may be used to enhance the fluorescence polarization signal. Proflavine (600 nM) was incubated with DNA (100 nM) and then next, $AgNO_3$ (200 nM) was added. In the absence of MnO_2 nanosheets, it was difficult to detect Ag^+ directly using the FP method, as the FP changed only from 51 ± 2 to 44 ± 1, namely the change in FP (ΔFP ~ 7) induced by the addition of Ag^+ was very weak. However, the addition of MnO_2 nanosheets (80 μg mL^{-1}) greatly increased the FP from 90 ± 5 to 196 ± 6, and the ΔFP (~100) was over 10 times higher than that without MnO_2 nanosheets (Fig. 2). This result showed that MnO_2 nanosheet can enhance the FP signal, and the MnO_2 nanosheet-assisted fluorescence polarization sensor was practicable for the detection of Ag^+.

3.3. Optimization of the concentration of MnO_2 nanosheets

The concentration of the MnO_2 nanosheets was further optimized for maximal enhancement of the detection signals. After proflavine (600 nM) was incubated with DNA (100 nM), various concentrations of MnO_2 nanosheets were added. As the concentration of MnO_2 nanosheets increased from 6.6 μg mL^{-1} to 100 μg mL^{-1}, the FP signals, both in the presence as well as absence of Ag^+, increased. Maximum ΔFP (~100) was obtained following the addition of 80 μg mL^{-1} MnO_2 nanosheets; therefore,

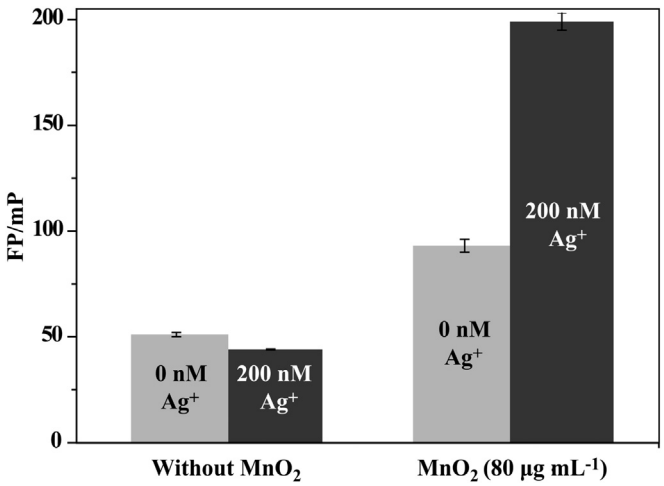

Fig. 2. Measurement of FP in the absence and presence of Ag^+ with/without the addition of MnO_2 nanosheets. All fluorescence polarization values were measured at least in triplicate.

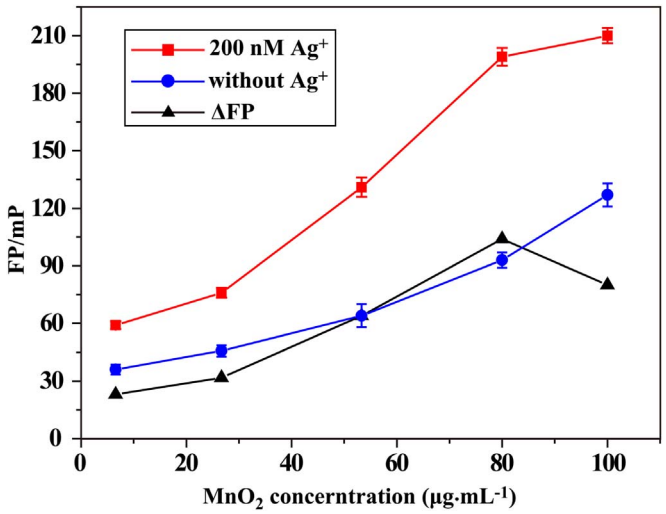

Fig. 3. Measurement of FP in the absence and presence of Ag^+ and various concentrations of MnO_2 nanosheets.

80 μg mL^{-1} was selected as the optimal concentration of MnO_2 nanosheets for the Ag^+ detection assay (Fig. 3).

3.4. Sensitivity and selectivity of Ag^+ detection

The sensitivity of this MnO_2 nanosheet-assisted fluorescence polarization method was evaluated using various concentrations of Ag^+. As the concentration of Ag^+ increased from 30 to 240 nM, the FP value of the interaction system increased from 97 ± 4 to 214 ± 4. A good linear response was observed between the concentration of Ag^+ (30–240 nM, namely 3.2–25.9 μg L^{-1}) and ΔFP (Fig. 4). The limit of detection (3σ) for Ag^+ was as low as ~9.1 nM (1 μg L^{-1}); this detection limit is comparable to those previously reported (Table S1, Supplementary material).

The selectivity of this method was evaluated by examining the FP response of the 11 other representative metal ions (Li^+, Mn^{2+}, Cd^{2+}, Ba^{2+}, Zn^{2+}, Ca^{2+}, Fe^{3+}, Mg^{2+}, Al^{3+}, Cu^{2+}, and Hg^{2+}). It could be observed that only Ag^+ can induce a significant ΔFP (99.2 ± 6). No significant change in FP was observed following the addition of these test ions (maximum of 8.1 ± 1 for Ca^{2+}), thereby demonstrating that this method shows high selectivity towards Ag^+ (Fig. 5).

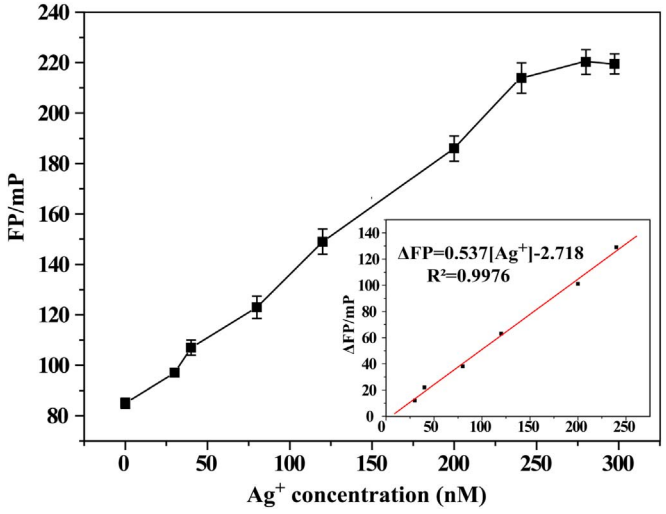

Fig. 4. Measurement of FP following the addition of various concentrations of Ag^+ in the presence of MnO_2 nanosheets (80 μg mL^{-1}); the inset shows the linear relationship between ΔFP and Ag^+ concentration.

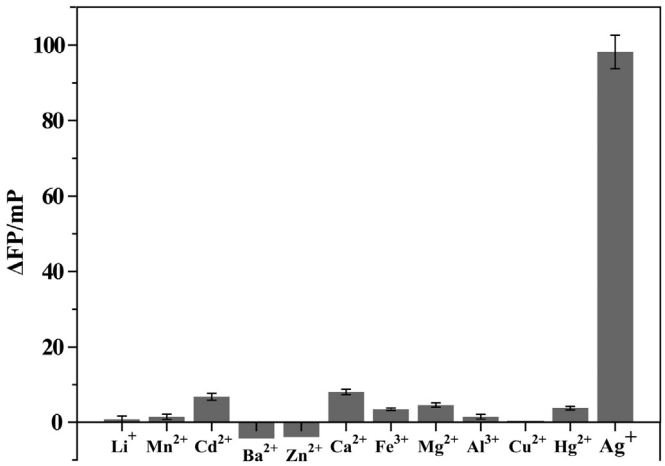

Fig. 5. Selectivity of Ag^+ detection; the relationship between ΔFP and 11 metal ions (200 nM).

According to the "Guidelines for drinking-water quality 4th ed." issued by WHO, a concentration of 100 μg L^{-1} for Ag^+ is permissible in drinking-water. Therefore, it can be inferred from the above results that the MnO_2 nanosheet-assisted fluorescence polarization method has adequate sensitivity and selectivity to be utilized for the detection of Ag^+ in environmental water samples.

3.5. Application to real samples

Hence, the practicability of this biosensor in detecting Ag^+ in real samples was further investigated. The average recoveries were in the range of 94.9–98.5% for the tap water and 93.4–105.7% for the lake water, with relative standard deviations (RSDs) of 2.3–4.6% (Table S2). The results proved that the biosensor can satisfy the practicability for the detection of Ag^+ in water samples.

3.6. The mechanism underlying changes in FP caused by the addition of Ag^+ in the presence of MnO_2 nanosheets

The DNA sequence utilized in the present study is in a single-stranded stem-loop structure. One T base was segregated by two bases (C and G) in the DNA duplex. Possible secondary structure of the DNA used in this study has been shown in Fig. 1. The interaction between Ag^+ and DNA was studied by CD experiments that examined the conformational changes in DNA upon binding of Ag^+. The positive peak for DNA alone at ~280 nm was found to disappear, and a new negative peak for DNA appeared at ~270 nm, as shown in Fig. 6a. This change in CD spectra was generally considered to indicate the formation of a C-Ag^+-C pair (Lin et al., 2011). Also, by comparing it with the CD spectra in Swasey's paper, the variation trend at 240–280 nm in CD spectra was speculated to be an indication of newly-formed G-Ag^+-G pairings. Therefore, it may be concluded that a conformational change occurred in DNA following the addition of Ag^+: some original C-G pairings were disrupted, and Ag^+-bridged C-C or G-G base pairings formed.

Another group of FP assays with the FAM-labeled same DNA (FAM-DNA) were carried out to further investigate the adsorption of DNA on the surface of MnO_2 nanosheets, before and after the addition of Ag^+. The FP value of FAM-DNA was found to exhibit a small increase following mixing with Ag^+. In the presence of MnO_2 nanosheets, the FAM-DNA-Ag^+ complex showed high FP compared with FAM-DNA alone (Fig. 6b), which demonstrated that the FAM-DNA-Ag^+ complex is more readily adsorbed on MnO_2 nanosheets than the latter. We speculate that the interaction of DNA with Ag^+ increases the positive charge of the former,

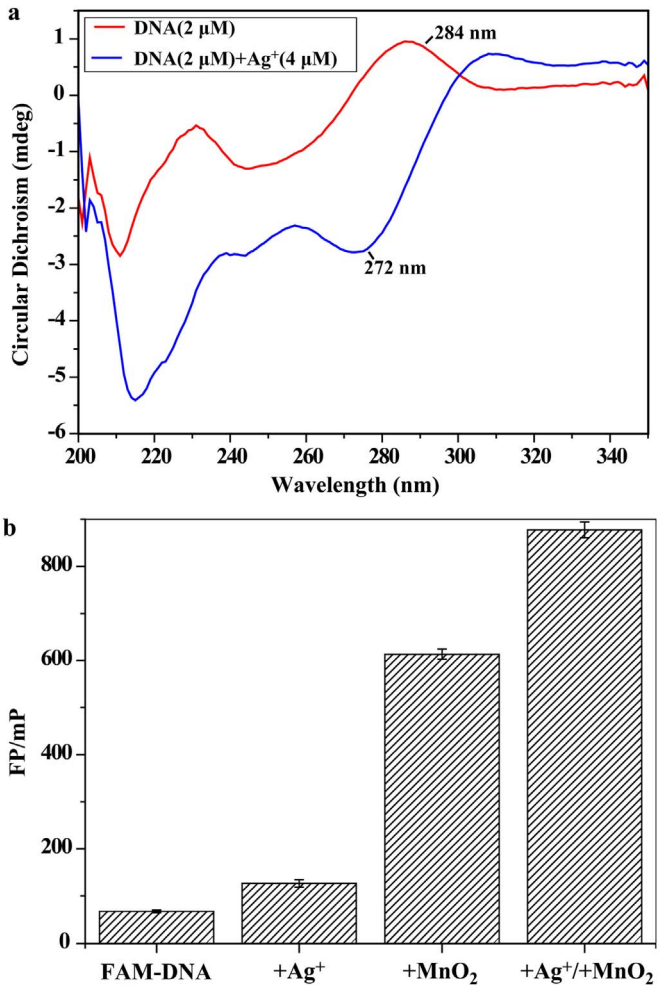

Fig. 6. (a) CD spectra of DNA in the absence and presence of Ag^+; (b) fluorescence polarization of FAM-DNA and FAM-DNA-Ag^+ complex in the absence and presence of MnO_2 nanosheets.

resulting in increased adsorption to the negatively charged surface of the MnO_2 nanosheets. Furthermore, in comparison with the proflavine-DNA complex without addition of Ag^+, the intercalation of proflavine into the DNA-Ag^+ complex enabled the latter to be more readily adsorbed on to the surface of MnO_2 nanosheets. This may additionally explain the increase in FP following the addition of Ag^+ to the proflavine-DNA complex.

Another DNA sequence "TGTTGTTGTTGTTAAAATTCTTCTTCTTC" was further tested. This one contains less C and G bases and no pairs according to the structure prediction. It turned out that the FP change for this sequence was weaker ($\sim 66.4 \pm 3$) than that of the proposed one (99.2 ± 6) after 200 nM Ag^+ was added. From the above results, it can be concluded that the existence of C and G bases in the DNA sequence is beneficial to improving the detection sensitivity for Ag^+ when using proflavine as an indicator.

4. Conclusions

In summary, a MnO_2 nanosheet-assisted ligand-DNA interaction-based fluorescence polarization method for sensitive detection of Ag^+ was designed in the present study. The role of MnO_2 nanosheets in assisting the measurement of fluorescence polarization was investigated. The exfoliated MnO_2 nanosheets were characterized and the performance parameters, such as detection limit, linearity and selectivity, were documented in order to validate the present method. The mechanism underlying the increase in fluorescence polarization, following the addition of Ag^+ in the presence of MnO_2 nanosheets, was investigated and discussed. Our findings demonstrate the feasibility of MnO_2 nanosheets in assisting the measurement of fluorescence polarization and that the present MnO_2 nanosheet-assisted fluorescence polarization biosensor represents a promising tool for the detection of Ag^+ ions in the environment. Overall, this nano MnO_2-based biosensor is low-cost and simple to complete determination assays. In addition, this strategy can be potentially applied to other types of molecular probes by simply changing the sequence of the ssDNA to a specific target.

Acknowledgments

L. Qi and Z. Yan contributed equally to this work and should be considered co-first authors. This work is financially supported by National Natural Science Foundation of China (No. 21275098), Natural Science Grand Research Program of Shaanxi Province (No. 2013SZS08-Z01), and Innovation Funds of Graduate Programs of Shaanxi Normal University (No. 2013CXS048).

Appendix A. Supplementary information

Supplementary data associated with this article can be found in the online version at doi:10.1016/j.bios.2016.08.093.

References

Choi, J.W., Kang, D.K., Park, H., deMello, A.J., Chang, S.I., 2012. Anal. Chem. 84, 3849–3854.
Cubrilovic, D., Zenobi, R., 2013. Anal. Chem. 85, 2724–2730.
DeJong, E.S., Chang, C.E., Gilson, M.K., Marino, J.P., 2003. Biochemistry 42, 8035–8046.
Gao, X.H., Lu, Y.Z., Zhang, R.Z., He, S.J., Ju, J., Liu, M.M., Li, L., Chen, W., 2015. J. Mater. Chem. C 3, 2302–2309.
He, D., He, X., Wang, K., Yang, X., Yang, X., Li, X., Zou, Z., 2014. Chem. Commun. 50, 11049–11052.
Huang, Y., Shi, M., Zhao, L.M., Zhao, S.L., Hu, K., Chen, Z.F., Chen, J., Liang, H., 2014. Biosens. Bioelectron. 54, 285–291.
Huang, Y., Zhao, S.L., Chen, Z.F., Shi, M., Liang, H., 2012. Chem. Commun. 48, 7480–7482.
Jang, H., Ryoo, S.R., Kim, Y.K., Yoon, S., Kim, H., Han, S.W., Choi, B.S., Kim, D.E., Min, D.H., 2013. Angew. Chem. Int. Ed. Engl. 52, 2340–2344.
Jiang, Y.L., Kong, W.W., Shen, Y.M., Wang, B.X., 2015. Tetrahedron 71, 5584–5588.
Kumar, M., Kumar, R., Bhalla, V., 2011. Org. Lett. 13, 366–369.
Kumar, V., Sengupta, A., Gavvala, K., Koninti, R.K., Hazra, P., 2014. J. Phys. Chem. B 118, 11090–11099.
Lai, C.Z., Fierke, M.A., Correa da Costa, R., Gladysz, J.A., Stein, A., Buhlmann, P., 2010. Anal. Chem. 82, 7634–7640.
Lee, J., Park, J., Hee Lee, H., Park, H., Kim, H.I., Kim, W.J., 2015. Biosens. Bioelectron. 68, 642–647.
Li, B., Du, Y., Dong, S., 2009. Anal. Chim. Acta 644, 78–82.
Lin, Z., Li, X., Kraatz, H.B., 2011. Anal. Chem. 83, 6896–6901.
Liu, S., Tian, J.Q., Wang, L., Sun, X.P., 2012. Sens. Actuators B – Chem. 165, 44–47.
Mensah, S.T., Gonzalez, Y., Calvo-Marzal, P., Chumbimuni-Torres, K.Y., 2014. Anal. Chem. 86, 7269–7273.
Morgan, T.P., Wood, C.M., 2004. Environ. Toxicol. Chem. 23, 1261–1267.
Murata, A., Harada, Y., Fukuzumi, T., Nakatani, K., 2013. Bioorg. Med. Chem. 21, 7101–7106.
Neidle, S., Pearl, L.H., Herzyk, P., Berman, H.M., 1988. Nucleic Acids Res. 16, 8999–9016.
Ono, A., Cao, S., Togashi, H., Tashiro, M., Fujimoto, T., Machinami, T., Oda, S., Miyake, Y., Okamoto, I., Tanaka, Y., 2008. Chem. Commun., 4825–4827.
Pang, Y.F., Rong, Z., Xiao, R., Wang, S.Q., 2015. Sci. Rep. 2015 (5), 9451.
Peng, L., Peng, X., Liu, B., Wu, C., Xie, Y., Yu, G., 2013. Nano Lett. 13, 2151–2157.
Qi, L., Huo, Y., Wang, H., Zhang, J., Dang, F.Q., Zhang, Z.Q., 2015. Anal. Chem. 87, 11078–11083.
Sakabe, M., Asanuma, D., Kamiya, M., Iwatate, R.J., Hanaoka, K., Terai, T., Nagano, T., Urano, Y., 2013. J. Am. Chem. Soc. 135, 409–414.
Shi, Y., Huang, W.T., Luo, H.Q., Li, N.B., 2011. Chem. Commun. 47, 4676–4678.
Sun, J., Yue, Y., Wang, P., He, H.L., Jin, Y.D., 2013. J. Mater. Chem. C 1, 908–913.
Swasey, S.M., Leal, L.E., Lopez-Acevedo, O., Pavlovich, J., Gwinn, E.G., 2015. Sci. Rep.

5, 10163.
Tan, Y., Zhang, X., Xie, Y.H., Zhao, R., Tan, C.Y., Jiang, Y.Y., 2012. Analyst 137, 2309–2312.
Tang, P., Juang, C.L., Harbison, G.S., 1990. Science 249, 70–72.
Umemoto, S., Im, S., Zhang, J.H., Hagihara, M., Murata, A., Harada, Y., Fukuzumi, T., Wazaki, T., Sasaoka, S., Nakatani, K., 2012. Chem. – Eur. J. 18, 9999–10008.
Wang, Y.L., Yuan, J.F., Shang, W., Zhang, J., Zhang, Z.Q., 2011. Analyst 136, 823–828.
Xu, G., Wang, G., Zhu, Y., Chen, L., He, X., Wang, L., Zhang, X., 2014. Biosens. Bioelectron. 59, 269–275.
Yang, Y., Liu, T., Cheng, L., Song, G., Liu, Z., Chen, M., 2015. ACS Appl. Mater. Interfaces 7, 7526–7533.
Yang, Y.Q., Kang, M.M., Fang, S.M., Wang, M.H., He, L.H., Feng, X.Z., Zhao, J.H., Zhang, Z.H., Zhang, H.Z., 2015b. J. Alloy. Compd. 652, 225–233.
Ye, B.C., Yin, B.C., 2008. Angew. Chem. Int. Ed. Engl. 47 (44), 8386–8389.
Yu, Y., Liu, Y., Zhen, S.J., Huang, C.Z., 2013. Chem. Commun. 49, 1942–1944.
Yuan, Y.X., Li, R.Q., Liu, Z.H., 2014a. Anal. Chem. 86, 3610–3615.
Yuan, Y.X., Wu, S.F., Shu, F., Liu, Z.H., 2014b. Chem. Commun. 50, 1095–1097.
Zhang, X.L., Zheng, C., Guo, S.S., Li, J., Yang, H.H., Chen, G., 2014. Anal. Chem. 86, 3426–3434.
Zhen, S.J., Yu, Y., Li, C.M., Huang, C.Z., 2015. Analyst 140, 353–357.
Zhu, C., Zeng, Z., Li, H., Li, F., Fan, C., Zhang, H., 2013. J. Am. Chem. Soc. 135, 5998–6001.
Zhu, G., Zhang, C.Y., 2014. Analyst 139, 6326–6342.